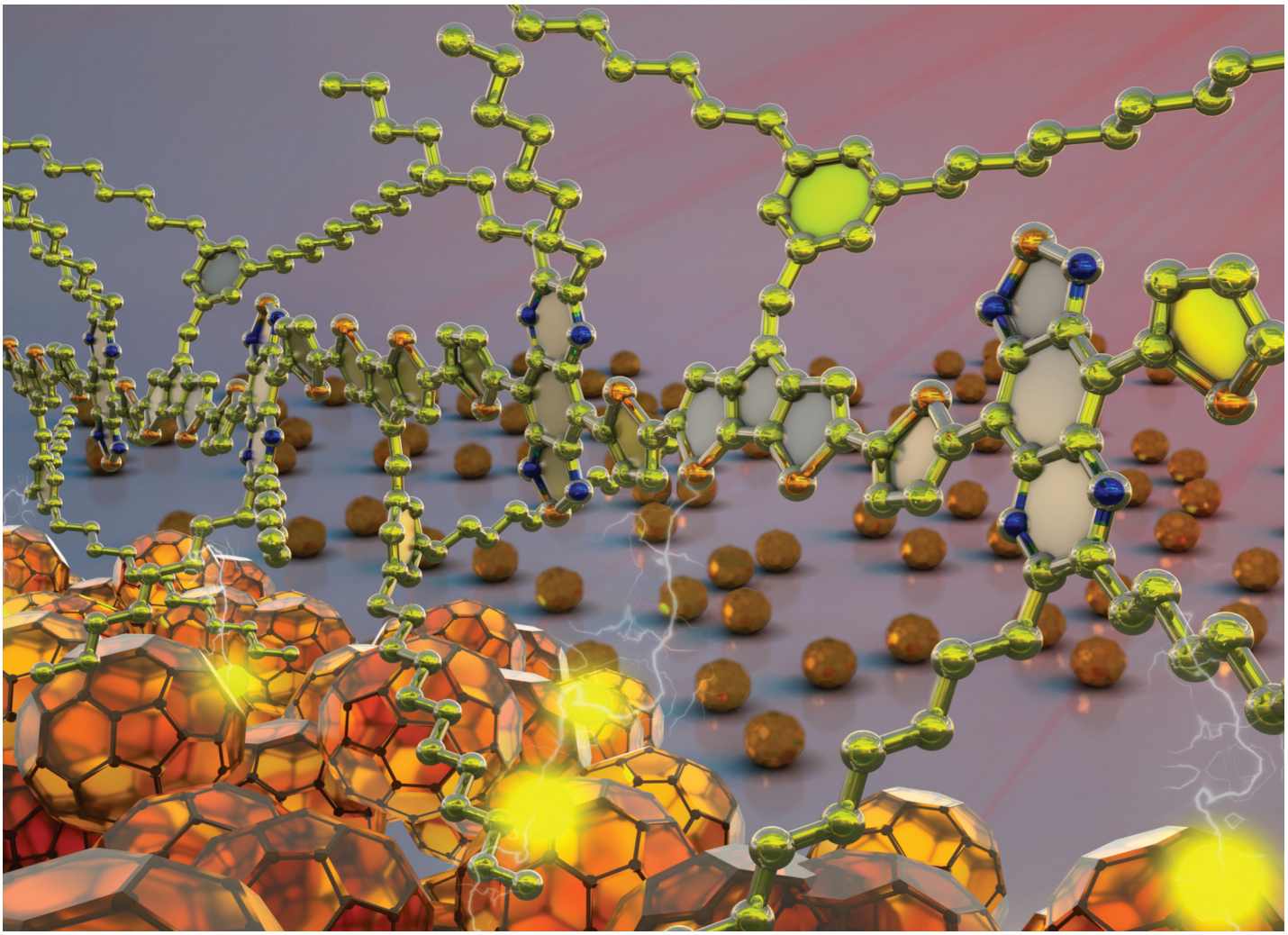

Highlighting research results from The School of Polymers and High Performance Materials at the University of Southern Mississippi.

Donor–acceptor polymers with tunable infrared photoresponse

Alexander E. London, Tse Nga Ng, Jason D. Azoulay, and co-workers demonstrate that exocyclic olefin substituted cyclopentadithiophene donors enable targeted engineering of the bandgap of photoresponsive donor–acceptor polymers at low energies. Bulk heterojunction photodiodes fabricated using these new materials demonstrate a detectivity (D^*) of > 10^{11} Jones within a spectral range of 0.6–1.43 μm and measurable D^* to 1.8 μm, the longest reported to date for conjugated polymer based systems.

As featured in:

See Jason D. Azoulay *et al.*, *Polym. Chem.*, 2017, **8**, 2922.

ROYAL SOCIETY OF CHEMISTRY

rsc.li/polymers

Registered charity number: 207890

Polymer Chemistry

PAPER

Cite this: *Polym. Chem.*, 2017, **8**, 2922

Donor–acceptor polymers with tunable infrared photoresponse†

Alexander E. London,[a] Lifeng Huang,[a] Benjamin A. Zhang,[a] M. Belén Oviedo,[b] Joshua Tropp,[a] Weichuan Yao,[c] Zhenghui Wu,[c] Bryan M. Wong,[b] Tse Nga Ng[c] and Jason D. Azoulay*[a]

Received 13th February 2017,
Accepted 16th March 2017

DOI: 10.1039/c7py00241f

rsc.li/polymers

Donor–acceptor (DA) conjugated polymers provide an important platform for the development of solution-processed optoelectronic devices. The complex interrelation between electronic properties and conformational disorder in these materials complicates the identification of design guidelines to control the bandgap at low energies, limiting the design of new optoelectronic and device functionalities. Here, we demonstrate that DA polymers comprised of exocyclic olefin substituted cyclopentadithiophene donors, in combination with conventional electron acceptors, display very narrow optical bandgaps (1.2 > E_g^{opt} > 0.7 eV) and primary photoexcitations extending into the shortwave infrared. Theoretical calculations reveal fundamental structure–property relationships toward bandgap and energy level control in these spectral regions. Bulk heterojunction photodiodes fabricated using these new materials demonstrate a detectivity (D^*) of > 10^{11} Jones within a spectral range of 0.6–1.43 μm and measurable D^* to 1.8 μm, the longest reported to date for conjugated polymer based systems.

Introduction

The inherent flexibility afforded by molecular design has accelerated the development of a wide variety of (opto)electronic technologies based on solution-processable organic semiconductors (OSCs). Donor–acceptor (DA) polymers comprised of alternating electron-rich (donor) and electron-poor (acceptor) moieties have emerged as the dominant class of high performance materials to date in organic photovoltaic (OPV) and photodetector (OPD) applications.[1] State-of-the-art OPDs, based on a bulk heterojunction (BHJ) architecture, have demonstrated a broad spectral response (0.3–1.45 μm), detectivities (D^*) > 10^{12} Jones (1 Jones = 1 cm $Hz^{0.5}$ W^{-1}), and a linear dynamic range over 100 dB in the visible sub-band (0.5 and 0.8 μm).[1e] There is significant interest in expanding the scope of these materials to improve functionality in the near-infrared (NIR: 0.9–1.4 μm) and extend utility into the shortwave IR (SWIR: 1.4–3 μm) to serve as alternatives to conventional inorganic semiconductor materials.[1g,2]

Unlike inorganic semiconductors, photoexcitation of OSCs does not lead to substantial instantaneous free carrier generation. Organic photoresponsive devices necessitate a lower ionization potential species (donor polymer) that manifests a singlet manifold transition ($S_0 \rightarrow S_1$) and possess a large intensity in the spectral region of interest. Photoexcitation results in bound electron–hole pairs (excitons), which require a suitable energy offset, facilitated by a higher electron affinity acceptor (typically a fullerene derivative, Fig. 1), to separate the exciton and drive charge transfer at the interface (heterojunction) between the two materials.[3] Dissociated charges are transported to their respective electrodes through interpenetrating bicontinuous donor and acceptor networks formed through nanoscale phase separation,[4] driven in part, by solubilizing substituents required for solution processing.[5] While general

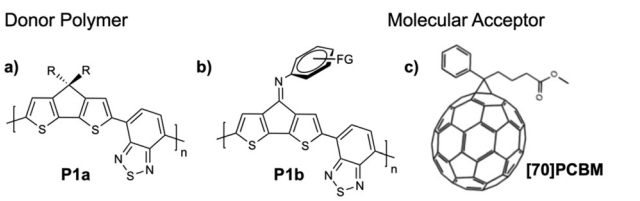

Fig. 1 Molecular structures of (a) poly[2,6-(4,4-bis(alkyl)-4*H*-cyclopenta[2,1-*b*;3,4-*b*']-dithiophene)-*alt*-4,7-(2,1,3-benzothiadiazole)] (PCPDTBT), (b) bridgehead imine substituted analog (**P1b**), where FG corresponds to a functional group, and (c) [6,6]-phenyl-C_{71}-butyric acid methyl ester ([70]PCBM).

[a]*School of Polymers and High Performance Materials, The University of Southern Mississippi, 118 College Drive #5050, Hattiesburg, Mississippi 39406, USA. E-mail: jason.azoulay@usm.edu*
[b]*Department of Chemical & Environmental Engineering and Materials Science & Engineering Program, University of California Riverside, Riverside, California 92521, USA*
[c]*Department of Electrical and Computer Engineering, 9500 Gilman Drive, University of California San Diego, La Jolla, California 92093, USA*

†Electronic supplementary information (ESI) available: Computational details and characterization data (PDF). See DOI: 10.1039/c7py00241f

design guidelines exist to tailor the HOMO–LUMO (highest occupied/lowest unoccupied molecular orbital) energies, absorption profiles, and transport characteristics of DA polymers, the complex interrelation between electronic properties and conformational disorder has precluded similar control at low energies.[6]

These complexities motivated our investigation of molecular design strategies that yield a reduction in bandgap and promote the appropriate properties suitable for long wavelength (λ) light detection in a conventional BHJ architecture. The prototypical narrow bandgap polymer PCPDTBT (**P1a**) is shown in Fig. 1. In combination with [6,6]-phenyl-C_{71}-butyric acid methyl ester ([70]PCBM), this material exhibits photoresponsivity extending into the NIR and high detectivities in solution-processed OPDs.[1f,7] Closely related bridgehead imine (*C*═NPh) substituted analogs (**P1b**) offer the advantage of systematic HOMO–LUMO modulation through varying electronic functionality on the phenyl (Ph) substituent.[8] This design motif also permits careful control of structural and electronic features necessary to overcome conjugation saturation behavior and achieve solution-processable DA polymers with very narrow optical bandgaps ($E_g^{opt} < 0.5$ eV).[9] It seemed reasonable that similar considerations should apply to copolymers comprised of bridgehead olefin (*C*═CPh) substituted cyclopentadithiophene (CPDT) structural units, with the advantage of increasing the LUMO energies of the resultant polymers to facilitate photoinduced electron transfer (PET) to conventional fullerene acceptors.[10,11]

Experimental

Materials and methods

All manipulations of air and/or moisture sensitive compounds were performed under an inert atmosphere using standard glove box and Schlenk techniques. Reagents, unless otherwise specified, were purchased from Sigma-Aldrich and used without further purification. Solvents (xylenes, THF, toluene, and ethanol) were degassed and dried over 4 Å molecular sieves. Deuterated solvents (C_6D_6, $CDCl_3$, and $C_2D_2Cl_4$) were purchased from Cambridge Isotope Labs and used as received. 3,5-Dibromobenzaldehyde and 4,7-dibromobenzo[*c*][1,2,5]thiadiazole were purchased from Oakwood Chemical and Sigma-Aldrich respectively, and purified by column chromatography prior to use. Tetrakis(triphenylphosphine)palladium(0) was purchased from Strem Chemicals and used as received. Alkylzinc halides were prepared according to a previously reported procedure.[9] 2,6-Dibromo-4*H*-cyclopenta[2,1-*b*:3,4-*b*′] dithiophene,[10d] 4,7-dibromobenzo[*c*][1,2,5]selenadiazole, 4,7-dibromo-[1,2,5]selenadiazolo[3,4-*c*]pyridine, 4,9-bis(5-bromothiophen-2-yl)-6,7-dioctyl-[1,2,5]thiadiazolo[3,4-*g*]quinoxaline, and 4,6-bis(5-bromo-2-thienyl)thieno[3,4-*c*][1,2,5]thiadiazole were prepared according to previously reported procedures.[12] ^{1}H and ^{13}C NMR spectra were collected on a Bruker Ascend 600 MHz spectrometer and chemical shifts, δ (ppm) were referenced to the residual solvent impurity peak of the given solvent. Data reported as: s = singlet, d = doublet, t = triplet, m = multiplet, br = broad; coupling constant(s), *J* are given in Hz. Flash chromatography was performed on a Teledyne Isco CombiFlash Purification System using Redi*Sep* Rf prepacked columns. Microwave assisted reactions were performed in a CEM Discover microwave reactor. Matrix-assisted laser desorption/ionization time-of-flight (MALDI-TOF) mass spectra were measured on a Bruker Microflex LT system. The number average molecular weight (M_n) and dispersity ($Đ$) were determined by gel permeation chromatography (GPC) relative to polystyrene standards at 160 °C in 1,2,4-trichlorobenzene (stabilized with 125 ppm of BHT) in an Agilent PL-GPC 220 High Temperature GPC/SEC system using a set of four PLgel 10 μm MIXED-B columns. Polymer samples were pre-dissolved at a concentration of 1.00–2.00 mg mL^{-1} in 1,2,4-trichlorobenzene with stirring for 4 h at 150 °C. Overlap of aromatic protons with solvent occurred in both $CDCl_3$ and C_6D_6 for compounds **1a**, **1b**, **2a**, and **2b**. The structures were confirmed using ^{13}C NMR and MALDI-TOF mass spectrometry.

UV-Vis-NIR spectroscopy

UV-Vis-NIR spectra were recorded using a Cary 5000 UV-Vis-NIR spectrophotometer. Thin films were prepared by spin coating a 10 mg mL^{-1} chlorobenzene (C_6H_5Cl) solution onto quartz substrates at 2000 rpm.

Electrochemistry

Electrochemical characteristics were determined by cyclic voltammetry (50 mV s^{-1}) carried out on drop-cast polymer films at room temperature in degassed anhydrous acetonitrile with tetrabutylammonium hexafluorophosphate (0.1 M) as the supporting electrolyte. The working electrode was a platinum wire, the counter electrode was a platinum wire and the reference electrode was Ag/AgCl. After each measurement the reference electrode was calibrated with ferrocene and the potential axis was corrected to the normal hydrogen electrode (NHE) using −4.75 eV for NHE.[7]

Device fabrication

Pre-patterned indium tin oxide (ITO) substrates were ultrasonically cleaned in detergent, deionized water and 2-propanol for 15 min sequentially. Polyethylenimine (PEIE) (35–40 wt%, 7000 g mol^{-1}, Sigma-Aldrich) was diluted with 2-methoxyethanol to achieve a concentration of 0.4 wt%. The diluted PEIE solution was spin coated onto the cleaned ITO substrate at 3500 rpm to form a film of ~10 nm, which was then annealed at 120 °C for 10 min in ambient conditions. For **P2**, the polymer and [70]PCBM (Osilla Ltd) in a 1 : 2 ratio were dissolved in anhydrous chlorobenzene : chloroform (3 : 1) at a polymer concentration of 14 mg mL^{-1}. For **P3**, the polymer and [70]PCBM (1 : 2) were dissolved in chlorobenzene : chloroform (2 : 1) at a polymer concentration of 15 mg mL^{-1}. The solutions were stirred at 45 °C overnight in a nitrogen atmosphere. 4% 1,8-diiodooctane (DIO) was added prior to spin coating **P3**. For **P4** and **P5**, the polymers (8.5 mg mL^{-1} and 7.5 mg mL^{-1}) were dissolved in chlorobenzene at 80 °C

overnight in a nitrogen atmosphere then filtered. [70]PCBM was added to give a solution with a 1 : 2 polymer : fullerene ratio and stirred at 80 °C for an additional 1 h. After this time, 3% DIO was added to the solution. The blend solutions were spin coated on the PEIE/ITO substrate at a spin speed of 1800, 1800, 700, and 300 rpm to form films with thicknesses of 175, 184, 385, and 255 nm for **P2**, **P3**, **P4**, and **P5** based devices, respectively. To complete the fabrication of the OPD, 15 nm MoO_3, followed by 100 nm Ag, was deposited on top of the blend film through thermal evaporation in a vacuum chamber at a pressure of 3×10^{-6} mbar. The effective areas of these photodetectors was 8.5 mm^2 (**P2**) and 9.0 mm^2 (**P3–P5**) measured with the help of an optical microscope. The devices were encapsulated between glass slides bonded with epoxy and subsequently characterized in air. The photodiode spectral response was amplified through a low-noise amplifier with an internal load resistor of 100 kΩ (for high gain) or 100 Ω (for low gain) and measured with a lock-in amplifier, using a monochromatic light source modulated by a mechanical chopper at a frequency of 390 Hz. Cutoff filters at 455 nm, 645 nm and 1025 nm were used to reduce the scattered light due to higher order diffraction. The lock-in amplifier can accurately measure a modulated photocurrent down to a magnitude of 2×10^{-11} A.

Synthesis and characterization

3,5-Didodecylbenzaldehyde (1a). In a nitrogen filled glove box, Pd-PEPPSI-IPr (0.274 g, 3.5 mol%) and 3,5-dibromobenzaldehyde (3.04 g, 11.5 mmol) were added to an oven-dried flask equipped with a stir bar. Toluene (30 mL) was added and the reaction mixture was stirred at room temperature to dissolve the contents. A THF solution (~0.50 M) of *n*-dodecylzinc bromide (81.0 mL, 40.3 mmol) was then added dropwise over a period of 30 min using a dropping funnel. After stirring for 16 h at room temperature, the reaction was heated to 60 °C and stirred at that temperature for 2 h. Upon cooling, the reaction mixture was quenched with saturated NH_4Cl (150 mL) and filtered through a Buchner funnel. The biphasic mixture was then poured into a separatory funnel, the water layer removed, and the organic phase washed with 3 × 100 mL 1 M Na_3EDTA (3 equiv. NaOH with EDTA), water (1 × 100 mL), and brine (1 × 100 mL). The organic solution was then dried with $MgSO_4$ and filtered through Celite. Volatiles were removed *in vacuo* and purification by flash chromatography on silica gel (hexanes to hexanes : ethyl acetate = 95 : 5 as the eluent) afforded a pale white solid (3.47 g, 68%). ^{1}H NMR (600 MHz, $CDCl_3$) δ 9.98 (1H, s), 7.51 (2H, s), 2.66 (4H, t, J = 7.8 Hz), 1.64 (4H, m), 1.40–1.20 (36H, m), 0.89 (6H, t, J = 6.7 Hz). ^{13}C NMR (151 MHz, $CDCl_3$) δ 192.95, 143.98, 136.82, 135.15, 127.29, 35.78, 32.07, 31.46, 29.82, 29.80, 29.72, 29.62, 29.57, 29.51, 29.42, 22.84, 14.25. MS (MALDI-TOF) m/z calculated for $C_{31}H_{54}O$: 442.42, found 442.61.

3,5-Ditetradecylbenzaldehyde (1b). In a nitrogen filled glove box, Pd-PEPPSI-IPr (0.277 g, 3.5 mol%) and 3,5-dibromobenzaldehyde (3.07 g, 11.6 mmol) were added to an oven-dried flask equipped with a stir bar. Toluene (30 mL) was added and the reaction mixture was stirred at room temperature to dissolve the contents. A THF solution (~0.50 M) of *n*-tetradecylzinc bromide (82.0 mL, 40.7 mmol) was then added dropwise over a period of 30 min using a dropping funnel. After stirring for 16 h at room temperature, the reaction was heated to 60 °C and stirred at that temperature for 2 h. Upon cooling, the reaction mixture was quenched with saturated NH_4Cl (150 mL) and filtered through a Buchner funnel. The biphasic mixture was then poured into a separatory funnel, the water layer removed, and the organic phase washed with 3 × 100 mL 1 M Na_3EDTA (3 equiv. NaOH with EDTA), water (1 × 100 mL), and brine (1 × 100 mL). The organic solution was then dried with $MgSO_4$ and filtered through Celite. Volatiles were removed *in vacuo* and purification by flash chromatography on silica gel (hexanes to hexanes : ethyl acetate = 95 : 5 as the eluent) afforded a colorless oil (4.06 g, 70%). ^{1}H NMR (600 MHz, $CDCl_3$) δ 9.97 (1H, s), 7.51 (2H, s), 2.66 (4H, t, J = 7.8 Hz), 1.64 (4H, m), 1.40–1.20 (44H, m), 0.89 (6H, t, J = 6.7 Hz). ^{13}C NMR (151 MHz, $CDCl_3$) δ 192.96, 143.97, 136.83, 135.13, 127.28, 35.78, 32.08, 31.46, 29.86, 29.84, 29.83, 29.81, 29.73, 29.62, 29.52, 29.42, 29.42, 22.84, 14.25. MS (MALDI-TOF) m/z calculated for $C_{35}H_{62}O$: 498.48, found 498.83.

2,6-Dibromo-4-(3,5-didodecylbenzylidene)-4*H*-cyclopenta-[2,1-*b*:3,4-*b*′]dithiophene (2a). Under nitrogen, sodium ethoxide (0.463 g, 6.80 mmol) was added to a suspension of 2,6-dibromo-4*H*-cyclopenta[2,1-*b*:3,4-*b*′]dithiophene (1.04 g, 3.09 mmol) in ethanol (10 mL) at 50 °C. After 30 min of stirring, a 50 °C solution of **1a** (1.37 g, 3.09 mmol) in ethanol (20 mL) was added dropwise. The reaction mixture was slowly heated and refluxed under nitrogen for 3 h. The reaction was then allowed to cool to room temperature, quenched with DI water (100 mL) and extracted with dichloromethane. The organic layer was washed with water (1 × 100 mL), brine (1 × 100 mL), and then dried with $MgSO_4$. After filtration through a Buchner funnel, volatiles were removed *in vacuo* and purification by flash chromatography (pentane as the eluent) yielded a red oil that solidified upon standing (1.67 g, 71%). ^{1}H NMR (600 MHz, C_6D_6) δ 7.23 (1H, s), 7.01 (2H, s), 6.83 (1H, s), 2.57 (4H, t, J = 7.8 Hz), 1.66 (4H, m), 1.47–1.21 (36H, m), 0.91 (6H, t, J = 6.7 Hz). ^{13}C NMR (151 MHz, C_6D_6) δ 145.18, 143.55, 140.58, 140.48, 136.69, 136.22, 132.04, 130.38, 130.05, 127.74, 126.48, 123.29, 111.46, 110.40, 36.31, 32.38, 32.06, 30.21, 30.16, 30.13, 30.12, 30.08, 29.87, 29.87, 23.16, 14.40. MS (MALDI-TOF) m/z calculated for $C_{40}H_{56}Br_2S_2$: 760.81, found 760.22.

2,6-Dibromo-4-(3,5-ditetradecylbenzylidene)-4*H*-cyclopenta [2,1-*b*:3,4-*b*′]dithiophene (2b). Under nitrogen, sodium ethoxide (0.453 g, 6.67 mmol) was added to a suspension of 2,6-dibromo-4*H*-cyclopenta[2,1-*b*:3,4-*b*′]dithiophene (1.02 g, 3.03 mmol) in ethanol (10 mL) at 50 °C. After 30 min of stirring, a 50 °C solution of **1b** (1.51 g, 3.03 mmol) in ethanol (20 mL) was added dropwise. The reaction mixture was slowly heated and refluxed under nitrogen for 3 h. The reaction was then allowed to cool to room temperature, quenched with DI water (100 mL) and extracted with dichloromethane. The organic layer was washed with water (1 × 100 mL), brine

(1 × 100 mL), and then dried with $MgSO_4$. After filtration through a Buchner funnel, volatiles were removed *in vacuo* and purification by flash chromatography (pentane as the eluent) yielded a red oil that solidified upon standing (1.51 g, 61%). ^{1}H NMR (600 MHz, C_6D_6) δ 7.24 (1H, s), 7.01 (2H, s), 6.83 (1H, s), 2.57 (4H, t, J = 7.8 Hz), 1.67 (4H, m), 1.47–1.21 (44H, m), 0.92 (6H, t, J = 6.7 Hz). ^{13}C NMR (151 MHz, C_6D_6) δ 145.18, 143.56, 140.59, 140.50, 136.71, 136.23, 132.04, 130.40, 130.05, 128.22, 128.06, 127.90, 127.74, 126.48, 123.29, 111.46, 110.41, 36.30, 32.37, 32.05, 30.22, 30.21, 30.21, 30.21, 30.16, 30.12, 30.06, 29.86, 29.85, 23.15, 14.39. MS (MALDI-TOF) m/z calculated for $C_{44}H_{64}Br_2S_2$: 816.47, found 816.28.

(4-(3,5-Didodecylbenzylidene)-4*H*-cyclopenta[2,1-*b*:3,4-*b*′] dithiophene-2,6-diyl)bis(trimethylstannane) (3a). In a nitrogen filled glove box, **2a** (0.995 g, 1.31 mmol), 5 equiv. $Me_3SnSnMe_3$ (2.14 g, 6.54 mmol), and $Pd(PPh_3)_4$ (0.0982 g, 8.50×10^{-2} mmol) were combined in a 35 mL microwave tube. The mixture was dissolved in approximately 25 mL of toluene. The tube was sealed, removed from the glove box and heated at 80 °C for 12 h. The reaction was allowed to cool and volatiles were removed *in vacuo.* The residue was extracted with hexanes, filtered, and poured into a separatory funnel containing 50 mL DI water. The organic layer was washed with DI water (3 × 50 mL), dried over anhydrous $MgSO_4$, and all volatiles removed *in vacuo*. Purification was accomplished by flash chromatography on reverse phase silica (ethanol containing 1% triethylamine as the eluent) affording a viscous red oil (0.862 g, 71%). ^{1}H NMR (600 MHz, C_6D_6, 298 K) δ 7.52 (1H, s), 7.42 (2H, s), 7.36 (1H, s), 7.30 (1H, s), 7.06 (1H, s), 2.64 (4H, t, J = 7.8 Hz), 1.70 (4H, m), 1.47–1.21 (36H, m), 0.92 (6H, t, J = 6.7 Hz), 0.31 (9H, s), 0.23 (9H, s). ^{13}C NMR (151 MHz, C_6D_6) δ 150.78, 147.29, 145.74, 143.29, 143.28, 137.52, 137.50, 136.41, 131.59, 131.14, 129.14, 129.13, 128.22, 128.06, 127.90, 36.43, 32.38, 32.15, 30.21, 30.21, 30.18, 30.16, 30.06, 30.02, 29.87, 23.16, 14.42, −8.30, −8.37. MS (MALDI-TOF) m/z calculated for $C_{46}H_{74}S_2Sn_2$: 928.33, found 928.12.

(4-(3,5-Ditetradecylbenzylidene)-4*H*-cyclopenta[2,1-*b*:3,4-*b*′] dithiophene-2,6-diyl)bis(trimethylstannane) (3b). In a nitrogen filled glove box, **2b** (0.940 g, 1.15 mmol), 5 equiv. $Me_3SnSnMe_3$ (1.88 g, 5.75 mmol), and $Pd(PPh_3)_4$ (0.0864 g, 7.48×10^{-2} mmol) were combined in a 35 mL microwave tube. The mixture was dissolved in approximately 25 mL of toluene. The tube was sealed, removed from the glove box and heated at 80 °C for 12 h. The reaction mixture was allowed to cool and volatiles were removed *in vacuo.* The residue was extracted with hexanes, filtered, and poured into a separatory funnel containing 50 mL DI water. The organic layer was washed with water (3 × 50 mL), dried over anhydrous $MgSO_4$, and all volatiles were removed *in vacuo*. Purification was accomplished by flash chromatography on reverse phase silica (ethanol containing 1% triethylamine as the eluent) affording a viscous red oil (0.839 g, 74%). ^{1}H NMR (600 MHz, C_6D_6, 298 K) δ 7.53 (1H, s), 7.43 (2H, s), 7.37 (1H, s), 7.31 (1H, s), 7.07 (1H, s), 2.64 (4H, t, J = 7.8 Hz), 1.70 (4H, m), 1.47–1.21 (44H, m), 0.92 (6H, t, J = 6.7 Hz), 0.31 (9H, s), 0.23 (9H, s). ^{13}C NMR (151 MHz, C_6D_6) δ 150.79, 147.30, 145.75, 143.30, 143.28, 137.53, 137.51, 136.44, 131.59, 131.15, 129.19, 129.14, 128.22, 128.06, 127.90, 36.43, 32.38, 32.15, 30.22, 30.19, 30.17, 30.13, 30.06, 30.01, 29.87, 23.16, 14.40, −8.32, −8.39. MS (MALDI-TOF) m/z calculated for $C_{50}H_{82}S_2Sn_2$: 984.39, found 984.12.

Synthesis of P1. A microwave tube was loaded with **3a** (150 mg, 0.162 mmol) and 4,7-dibromobenzo[*c*][1,2,5]thiadiazole (45.4 mg, 0.154 mmol). The tube was brought inside a glove box and approximately 6.5 mg of $Pd(PPh_3)_4$ and 750 μL of xylenes were added. The tube was sealed and subjected to the following reaction conditions in a microwave reactor: 120 °C for 5 min, 140 °C for 5 min and 170 °C for 40 min. After this time the reaction was allowed to cool leaving a solid gelled material. The mixture was precipitated into methanol and collected *via* filtration. The residual solid was loaded into an extraction thimble and washed successively with methanol (4 h), acetone (4 h), hexanes (12 h), hexanes : THF (3 : 1) (12 h), and again with acetone (2 h). The polymer was dried *in vacuo* to give 81 mg (67%) of a blue solid. GPC (160 °C, 1,2,4-trichlorobenzene) M_n = 8.0 kg mol^{-1}, $Đ$ = 1.21. λ_{max} (solution, $CHCl_3$, 25 °C)/nm 812 (ε/L mol^{-1} cm^{-1} 18 161); λ_{max} (thin film)/nm 893. ^{1}H NMR (600 MHz, $C_2D_2Cl_4$, 398 K) δ 8.55–6.35 (8H, br m), 3.35–2.51 (4H, br), 2.30–0.85 (46H, br).

Synthesis of P2. A microwave tube was loaded with **3a** (150 mg, 0.162 mmol) and 4,7-dibromobenzo[*c*][1,2,5]selenadiazole (52.6 mg, 0.154 mmol). The tube was brought inside a glove box and approximately 6.5 mg of $Pd(PPh_3)_4$ and 750 μL of xylenes were added. The tube was sealed and subjected to the following reaction conditions in a microwave reactor: 120 °C for 5 min, 140 °C for 5 min and 170 °C for 40 min. After this time the reaction was allowed to cool leaving a solid gelled material. The mixture was precipitated into methanol and collected *via* filtration. The residual solid was loaded into an extraction thimble and washed successively with methanol (4 h), acetone (4 h), hexanes (12 h), hexanes : THF (3 : 1) (12 h), and again with acetone (2 h). The polymer was dried *in vacuo* to give 89 mg (71%) of a green solid. GPC (160 °C, 1,2,4-trichlorobenzene) M_n = 10.1 kg mol^{-1}, $Đ$ = 2.90. λ_{max} (solution, $CHCl_3$, 25 °C)/nm 878 (ε/L mol^{-1} cm^{-1} 19 073); λ_{max} (thin film)/nm 927. ^{1}H NMR (600 MHz, $C_2D_2Cl_4$, 398 K) δ 8.55–6.25 (8H, br m), 3.43–2.43 (4H, br m), 2.27–0.81 (46H, br).

Synthesis of P3. A microwave tube was loaded with **3a** (150 mg, 0.162 mmol) and 4,7-dibromo-[1,2,5]selenadiazolo-[3,4-*c*]pyridine (52.7 mg, 0.154 mmol). The tube was brought inside a glove box and approximately 6.5 mg of $Pd(PPh_3)_4$ and 750 μL of xylenes were added. The tube was sealed and subjected to the following reaction conditions in a microwave reactor: 120 °C for 5 min, 140 °C for 5 min and 170 °C for 40 min. After this time the reaction was allowed to cool leaving a solid gelled material. The mixture was precipitated into methanol and collected *via* filtration. The residual solid was loaded into an extraction thimble and washed successively with methanol (4 h), acetone (4 h), hexanes (12 h), hexanes : THF (3 : 1) (12 h), and again with acetone (2 h). The polymer was dried *in vacuo* to give 83 mg (66%) of a green solid. GPC (160 °C, 1,2,4-trichlorobenzene) M_n = 13.2 kg mol^{-1}, $Đ$ = 1.64. λ_{max} (solution, $CHCl_3$, 25 °C)/nm 883

(ε/L mol^{-1} cm^{-1} 14 260); λ_{max} (thin film)/nm 911. ^{1}H NMR (600 MHz, $C_2D_2Cl_4$, 398 K) δ 8.75–6.20 (7H, br m), 3.40–2.53 (4H, br m), 2.52–0.79 (46H, br).

Synthesis of P4. A microwave tube was loaded with **3a** (150 mg, 0.162 mmol) and 4,9-bis(5-bromothiophen-2-yl)-6,7-dioctyl-[1,2,5]thiadiazolo[3,4-*g*]quinoxaline (113 mg, 0.154 mmol). The tube was brought inside a glove box and approximately 6.5 mg of $Pd(PPh_3)_4$ and 750 μL of xylenes were added. The tube was sealed and subjected to the following reaction conditions in a microwave reactor: 120 °C for 5 min, 140 °C for 5 min and 170 °C for 50 min. After this time the reaction was allowed to cool leaving a solid gelled material. The mixture was precipitated into methanol and collected *via* filtration. The residual solid was loaded into an extraction thimble and washed successively with methanol (4 h), acetone (4 h), hexanes (12 h), THF (12 h), and again with acetone (2 h). The polymer was dried *in vacuo* to give 153 mg (80%) of a black solid. GPC (160 °C, 1,2,4-trichlorobenzene) M_n = 18.8 kg mol^{-1}, $Đ$ = 1.91. λ_{max} (solution, $CHCl_3$, 25 °C)/nm 1073 (ε/L mol^{-1} cm^{-1} 34 009); λ_{max} (thin film)/nm 1079. ^{1}H NMR (600 MHz, $C_2D_2Cl_4$, 398 K) δ 9.31–6.25 (10H, br m), 3.30–2.45 (8H, br m), 2.46–0.75 (76H, br).

Synthesis of P5. A microwave tube was loaded with **3b** (150 mg, 0.152 mmol) and 4,6-bis(5-bromo-2-thienyl)thieno[3,4-*c*][1,2,5]thiadiazole (67.2 mg, 0.145 mmol). The tube was brought inside a glove box and approximately 6.5 mg of $Pd(PPh_3)_4$ and 750 μL of xylenes were added. The tube was sealed and subjected to the following reaction conditions in a microwave reactor: 120 °C for 5 min, 140 °C for 5 min and 170 °C for 30 min. After this time the reaction was allowed to cool leaving a solid gelled material. The mixture was precipitated into methanol and collected *via* filtration. The residual solid was loaded into an extraction thimble and washed successively with methanol (4 h), acetone (4 h), hexanes (12 h), THF (12 h), and again with acetone (2 h). The polymer was dried *in vacuo* to give 109 mg (74%) of a purple solid. GPC (160 °C, 1,2,4-trichlorobenzene) M_n = 14.4 kg mol^{-1}, $Đ$ = 1.64. λ_{max} (solution, $CHCl_3$, 25 °C)/nm 963 (ε/L mol^{-1} cm^{-1} 22 843); λ_{max} (thin film)/nm 967. ^{1}H NMR (600 MHz, $C_2D_2Cl_4$, 398 K) δ 8.55–6.25 (10H, br m), 3.25–2.43 (4H, br m), 2.50–0.51 (54H, br).

Results and discussion

Fig. 2 displays the copolymer structures considered in this study. DA polymers comprised of a *C*═CPh substituted CPDT donor (R, R′ = CH_3 for theoretical examination) and acceptors based on 2,1,3-benzothiadiazole (BT, **P1**), 2,1,3-benzoselenadiazole (BSe, **P2**), pyridal[2,1,3]selenadiazole (PSe, **P3**), thiophene flanked [1,2,5]thiadiazolo[3,4-*g*]quinoxaline (TQ, **P4**), and thiophene flanked thieno[3,4-*c*][1,2,5]thiadiazole (TT, **P5**), were theoretically examined on the basis of incorporating design elements anticipated to lead to progressive bandgap narrowing.[7a,12] The optimized ground-state (S_0) structures, electronic properties, and lowest excited-state (S_1) energies of **P1–P5** were calculated with density functional theory (DFT) and time-dependent DFT, respectively, at the B3LYP/6-31G(d) level of theory.[13] The HOMO and LUMO wavefunctions of **P1**, **P4** and **P5** are highlighted in Fig. 2 (n = 4 shown for clarity). **P2** and **P3** display similar structural and nodal characteristics to **P1** and are highlighted in Fig. S1–S4 in the ESI.†

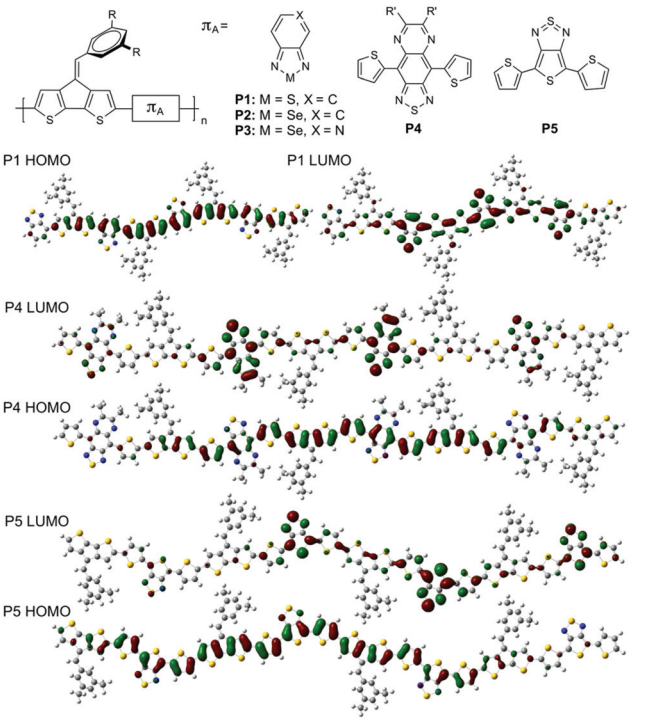

Fig. 2 Copolymer structures considered in this study. Optimized ground-state (S_0) geometric structures for **P1**, **P4**, and **P5**, and pictorial representations of the HOMO and LUMO wavefunctions as determined at the B3LYP/6-31G(d) level of theory.

The comparatively lower bandgap of **P1** (E_g^{DFT} = 1.34 eV) relative to **P1a** and **P1b** (E_g^{DFT} = 1.56 eV and 1.47 eV, respectively) can be ascribed to planarization of the CPDT core (in contrast to the modest curvature of *C*, Si, and *C*═NPh substituted analogs),[8a,12f] and a reduction in the overall bond length alternation (see Fig. S5, ESI†).[14] **P1** is highly planar with negligible rotational disorder (donor/acceptor dihedral angle = 179.36°), which contributes to extended electron delocalization.[13a] Solubilizing substituents are oriented nearly orthogonal and situated at a site remote to the polymer backbone in **P1**. Collectively, these structural features are likely to permit improved π-interactions, further mitigate backbone torsion, and increase resilience toward conjugation saturation behavior.[15] The lowest vertical excitation energy (E_g^{vert}), which more appropriately approximates the onset of optical absorption, was obtained through extrapolation of a series of oligomers (n = 1–6) to $n \rightarrow \infty$ and fitting the data to the Kuhn equation.[16] In moving across the series we note a progressive narrowing of E_g^{vert}: **P1** = 1.04 eV; **P2** = 0.94 eV; **P3** = 0.88 eV; **P4** = 0.68 eV; **P5** = 0.63 eV, illustrating iterative control throughout the NIR and extension into the SWIR. Structural and electronic characteristics associated with *C*═CPh substitution manifest in other

donor/heterocyclic acceptor configurations (**P4** and **P5**). As in several other similar materials, the HOMO is delocalized over the whole π-system and the LUMO is more localized on the acceptor. The spectra of the (**P1–P5**)$_6$ oligomers exhibit one dominant $S_0 \rightarrow S_1$ transition of HOMO → LUMO character with large oscillator strengths, consistent with DA polymers commonly utilized in photoresponsive devices (see ESI† for full details).[13b]

Bandgap engineering at low energies will require careful chemical, electronic, and structural control. Modular side-chain engineering approaches are also necessary owing to the immense difficulty in achieving the appropriate phase characteristics associated with polymers[6a] and heterojunction blends.[17] To address these challenges, we developed a synthetic route amenable to systematic structural and electronic variation as depicted in Scheme 1. Linear (R = $C_{12}H_{25}$ and $C_{14}H_{29}$) solubilizing groups were introduced into the 3,5-positions of the Ph ring to minimize backbone torsion and promote solubility. The coupling of dodecylzinc bromide and tetradecylzinc bromide with 3,5-dibromobenzaldehyde was accomplished using a Pd-PEPPSI-IPr pre-catalyst. Optimization of the solvent system (toluene/THF = 1 : 3), catalyst loading (3.5%), and heating of the reaction mixture ensured high conversions, providing the coupled products (**1a** and **1b**) in overall yields > 60% in the presence of the aldehyde functionality. The reaction of **1a** and **1b** with 2,6-dibromo-4*H*-cyclopenta[2,1-*b*:3,4-*b*′]dithiophene using sodium ethoxide (NaOEt) in ethanol (EtOH) affords the desired *C*=CPh substituted CPDT donors (**2a** and **2b**) in 71% and 61% yield.[18] Reaction with 5 equiv. of hexamethylditin ($Me_3SnSnMe_3$) using $Pd(PPh_3)_4$ in toluene affords the bis-trimethylstannyl donors (**3a** and **3b**) in > 70% yields.

Copolymerization of **3a** with 4,7-dibromobenzo[*c*][1,2,5]-thiadiazole (**P1**), 4,7-dibromobenzo[*c*][1,2,5]selenadiazole (**P2**), 4,7-dibromo-[1,2,5]selenadiazolo[3,4-*c*]pyridine (**P3**) 4,9-bis (5-bromothiophen-2-yl)-6,7-dioctyl-[1,2,5]thiadiazolo[3,4-*g*] quinoxaline (**P4**), and **3b** with 4,6-bis(5-bromo-2-thienyl)thieno [3,4-*c*][1,2,5]thiadiazole (**P5**) was carried out *via* microwave heating using $Pd(PPh_3)_4$ (3.5 mol%) as the catalyst in xylenes.[7a,12] This results in the rapid formation of polymers in reaction times < 60 minutes and isolated yields of 65–80% after purification by soxhlet extraction. **P4** (R = $C_{12}H_{25}$, R′ = C_8H_{17}) and **P5** (R = $C_{14}H_{29}$) required additional solubilizing units to promote solubility of the extended π-systems in common organic solvents used for solution processing. Gel permeation chromatography (GPC) at 160 °C in 1,2,4-trichlorobenzene showed number average molecular weights (M_n) ~8–19 kg mol^{-1} ensuring > 10 repeat units to allow a comparison between experiment and theory, albeit well below typical high performance materials.

Absorption spectra of **P1–P5** at 25 °C in chloroform ($CHCl_3$) and as thin-films are shown in Fig. 3. Broad absorption profiles that peak in the NIR (λ_{max} = 0.89–1.08 μm) with electronic transitions extending into the SWIR (~1.8 μm) are evident. In transitioning from $CHCl_3$ at 25 °C to the solid state, λ_{max} and the onset of optical absorption exhibit a bathochromic shift highly dependent on the structure of the polymer, indicating intermolecular interactions in the solid state. The optical bandgap (E_g^{opt}) of **P1** is ~1.1 eV, as estimated from the absorption onset of the thin film. Cyclic voltammetry (CV) is widely utilized to determine the frontier orbital energy levels of the donor and acceptor components in organic photoresponsive devices.[19] CV shows that the HOMO is located at −5.01 eV and the LUMO at −3.65 eV, as determined by the oxidation and reduction onset, respectively.[7] This gives an electrochemical bandgap (E_g^{elec}) of 1.36 eV, in excellent agreement with theory (E_g^{DFT} = 1.34 eV). We note an increase in the HOMO and stabilization of the LUMO relative to **P1a** (R = $C_{12}H_{25}$; E_{HOMO} = −5.33 eV; E_{LUMO} = −3.52 eV, E_g^{elec} of 1.81 eV).[7a] Comparison with the corresponding *C*=NPh substituted analog shows an increase in both the HOMO–LUMO energies and overall narrowing of the bandgap (**P1b**: Ph = 3,5-$C_{12}H_{25}$; E_{HOMO} = −5.40 eV; E_{LUMO} = −3.96 eV, E_g^{elec} of 1.44 eV).[9]

Substitution of BT for BSe (**P2**), wherein a single atom in the benzochalcogenodiazole unit is varied from sulfur (S) to selenium (Se), results in red-shifted absorption profile (λ_{max} = 0.93 μm) with measurable absorbance extending to λ > 1.4 μm in the solid state. The electrochemical characteristics reflect a

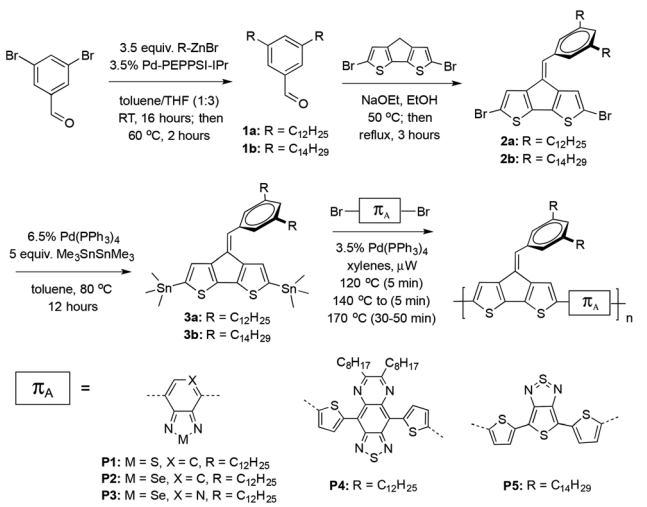

Scheme 1 Synthesis of **P1–P5**.

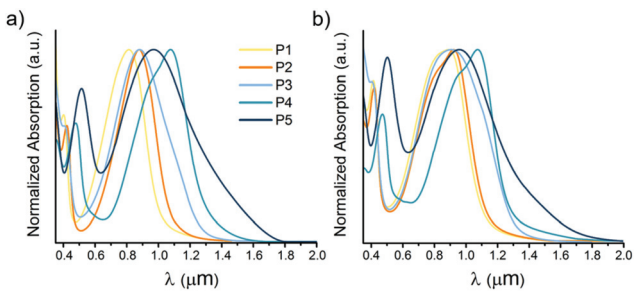

Fig. 3 (a) Absorption spectra of **P1–P5** at 25 °C in $CHCl_3$ and (b) as thin films.

modest reduction in the LUMO energy (E_{HOMO} = −5.01 eV; E_{LUMO} = −3.75 eV; E_g^{elec} of 1.26 eV). A further reduction is obtained by incorporating a PSe analog (**P3**), resulting in higher electron affinity in the backbone and a narrower bandgap (E_g^{opt} = 0.94 eV). A pronounced bathochromic shift is evident in transitioning to the solid state in **P3**, leading to measurable absorbance extending to λ > 1.6 μm. It should be noted that the PSe for BSe substitution also reduces the symmetry of the repeat unit, which may account for the broad spectral features. Electrochemical measurements are consistent with a reduction in both the HOMO–LUMO energies (E_{HOMO} = −5.10 eV; E_{LUMO} = −3.95 eV; E_g^{elec} of 1.15 eV).

Heteroannulated variants of BT, such as thiadiazoloquinoxaline (TQ) result in a significant reduction in the LUMO,[20] which can be mitigated by the presence of thiophene spacers.[13a] A further narrowing of the bandgap was obtained in **P4** (λ_{max} = 1.08 μm) with measurable absorbance extending to λ > 1.6 μm in the solid state. A plot of absorbance squared (Fig. S11†) is consistent with low energy excitations at these wavelengths and E_g^{opt} ~0.85 eV (1.46 μm). The pronounced absorption shoulder and similar spectral profiles in solution and the solid state are consistent with strong intermolecular interactions in **P4**. Substitution of the TQ-based acceptor with a thiophene flanked thieno[3,4-*c*][1,2,5]thiadiazole heterocycle results in a further redshift consistent with theoretical predictions (**P5**: E_{HOMO} = −4.85 eV; E_{LUMO} = −3.95 eV; E_g^{elec} of 0.90 eV; E_g^{opt} ~0.74 eV). The utility of bridgehead *C*═CPh substitution in mitigating conjugation saturation behavior is evident in view of values for E_g^{elec} and E_g^{opt} that are similar with those from theory (E_g^{DFT} and E_g^{vert}), compared in Table 1. **P1–P5** retain the appropriate difference in electrochemical potential relative to common fullerene acceptors, such as [60]PCBM and [70]PCBM (LUMO ~−4.2 and −4.3 eV, respectively), providing the necessary driving force needed for efficient charge separation.

To demonstrate the ultimate utility of copolymers based on *C*═CPh substitution, BHJ photodetectors were fabricated using **P2–P5** in combination with [70]PCBM. The device test structure of the photodiode is shown in Fig. 4a and was used for screening purposes in the absence of significant optimization. The fabrication and measurement procedures were carried out as previously reported.[21] Based on the energy level

Table 1 Optical, electrochemical, and calculated properties of **P1–P5**

	λ_{max} [a] (μm)	E_g^{opt} [b] [eV]	E_g^{vert} [eV]	E_{HOMO}/E_{LUMO} [c] [eV]	E_g^{elec} [d] [eV]	E_g^{DFT} [e] [eV]
P1	0.89	1.11	1.04	−5.01/−3.65	1.36	1.34
P2	0.93	1.08	0.94	−5.01/−3.75	1.26	1.24
P3	0.91	0.94	0.88	−5.10/−3.95	1.15	1.12
P4	1.08	0.85	0.68	−4.80/−3.66	1.14	0.91
P5	0.97	0.74	0.63	−4.85/−3.95	0.90	0.88

[a] Films spin coated from a C_6H_5Cl solution (10 mg mL^{-1}). [b] Estimated from the absorption onset of the film. [c] E_{HOMO} calculated from the onset of oxidation, E_{LUMO} calculated from the onset of reduction. [d] E_g^{elec} calculated from the difference between E_{HOMO} and E_{LUMO}. [e] HOMO/LUMO orbital energy gap (E_g^{DFT}).

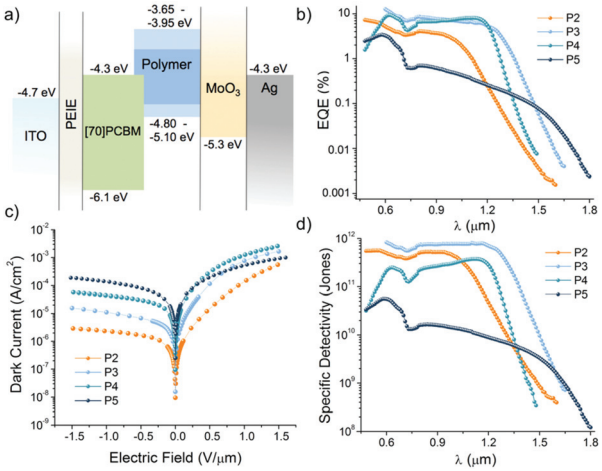

Fig. 4 (a) Energy diagram of the ITO/PEIE/polymer:[70]PCBM/MoO_3/Ag photodiode. (b) External quantum efficiency, (c) current–voltage (*I–V*) characteristics measured in the dark, and (d) detectivity of polymer photodetectors.

diagram in Fig. 4a, charge separated carriers can be efficiently generated by PET and subsequently transported *via* the BHJ nanomorphology to opposite electrodes. The low work function of 80% ethoxylated polyethylenimine (PEIE) modified indium tin oxide (ITO) favors the collection of electrons at the cathode.[22] MoO_3 is used as the electron blocking layer at the anode.[23] From initial examination, the devices in Fig. 4b show external quantum efficiencies (EQEs) similar to previously reported narrow bandgap organic devices demonstrating that photons absorbed by **P2–P5** contribute to the photocurrent.[1e,24] Spectrally resolved NIR-SWIR EQEs of 4%, 7%, 6%, and 0.2% were measured at λ = 0.90, 1.10, 1.20, and 1.35 μm for **P2**, **P3**, **P4**, and **P5** based devices, respectively. We note that devices based on the **P5**:[70]PCBM combination generally resulted in poor film quality when compared to **P2–P4** devices.

The specific detectivity (D^*) is the main figure of merit that takes both dark current (Fig. 4c) and EQE (Fig. 4b) into account. It is defined as: $D^* = (A\Delta f)^{1/2}R/i_n$, where $R = J_{photo}/P_{illumin}$ is the responsivity related to EQE, A is the effective photodetector area, Δf is the electrical bandwidth, and i_n is the noise current measured in the dark. In **P2** devices, peak specific detectivities at zero bias, where $D^* > 10^{11}$ Jones are obtained in the region of maximum absorption ($0.6 < \lambda < 1.1$ μm). At λ_{max}, $D^* = 5 \times 10^{11}$ Jones is obtained with measurable photocurrent spanning the range of absorption ($D^* = 1 \times 10^{10}$ Jones at λ = 1.3 μm). **P3** devices exhibit $D^* > 10^{11}$ Jones within a range of $0.6 < \lambda < 1.3$ μm, $D^* = 2 \times 10^{11}$ Jones at λ = 1.33 μm, and $D^* > 1 \times 10^{10}$ Jones at λ = 1.5 μm. Addition of [70]PCBM alters the absorption spectra of **P3** (Fig. S13†), leading to a bathochromic shift and increased photocurrent at longer λ. **P4** devices operate between $0.6 < \lambda < 1.5$ μm with $D^* = 3 \times 10^{11}$ Jones at λ_{max} = 1.2 μm. We note that D^* obtained for devices based on **P3** and **P4**, in the absence of optimization, are greater than fused porphyrins ($D^* = 1.6 \times 10^{11}$ Jones at λ = 1.09 μm and 2.3×10^{10} Jones at λ = 1.35 μm)[24a] and are com-

parable to cooled PbS detectors in this range.[2a] **P5** devices exhibit $D^* > 10^9$ Jones within a range of $0.6 < \lambda < 1.65$ μm, with measurable photocurrent spanning the range of absorption ($D^* = 1.2 \times 10^8$ Jones at $\lambda = 1.8$ μm). The photocurrent generation of **P5** spans the technologically relevant region from 1–1.8 μm, traditionally accomplished using alloys of $Ga_xIn_{1-x}As$. Fig. 4d demonstrates a progressive increase in the dark current as the bandgap is narrowed potentially limiting D^* obtained with the **P5**:[70]PCBM combination, but pointing toward improvements associated with material and device optimization.

Conclusions

These results demonstrate detection of longer λ light than was previously possible using OSCs and highlight the potential of tunable NIR-SWIR photoresponsive DA polymers that can be applied in a variety of photodetection applications traditionally limited to inorganic semiconductors, colloidal quantum dots, and carbon nanotubes. From a broader perspective, more precise narrow bandgap DA polymers will enable targeted engineering of the bandgap at low energies, the generation of materials for fundamental studies, and enable new functionality in the IR spectral regions.

Acknowledgements

Financial support was provided by the University of Southern Mississippi start-up funds, UCSD ECE start-up funds, and the National Science Foundation (NSF OIA-1632825). A. E. L. and J. T. acknowledge support from the NSF (DGE-1449999). W. Y., Z. W., and T. N. N. acknowledge support from the NSF (CMMI-1635729). M. B. O. and B. M. W. acknowledge support from the UC Riverside Collaborative Seed Grant Portions of this research were carried out at the Molecular Foundry, Lawrence Berkeley National Laboratory, which was supported by the Office of Science, Office of Basic Energy Sciences, of the US Department of Energy under Contract no. DE-AC02-05CH11231.

References

1 (*a*) G. Li, R. Zhu and Y. Yang, *Nat. Photonics*, 2012, **6**, 153–161; (*b*) S. Zhang, L. Ye and J. Hou, *Adv. Energy Mater.*, 2016, **6**, 1502529; (*c*) J. Qi, J. Han, X. Zhou, D. Yang, J. Zhang, W. Qiao, D. Ma and Z. Y. Wang, *Macromolecules*, 2015, **48**, 3941–3948; (*d*) H. Yao, L. Ye, H. Zhang, S. Li, S. Zhang and J. Hou, *Chem. Rev.*, 2016, **116**, 7397–7457; (*e*) X. Gong, M. Tong, Y. Xia, W. Cai, J. S. Moon, Y. Cao, G. Yu, C. L. Shieh, B. Nilsson and A. J. Heeger, *Science*, 2009, **325**, 1665–1667; (*f*) X. Gong, M. H. Tong, S. H. Park, M. Liu, A. Jen and A. J. Heeger, *Sensors*, 2010, **10**, 6488–6496; (*g*) K. J. Baeg, M. Binda, D. Natali, M. Caironi and Y. Y. Noh, *Adv. Mater.*, 2013, **25**, 4267–4295; (*h*) R. D. Jansen-van Vuuren, A. Armin, A. K. Pandey, P. L. Burn and P. Meredith, *Adv. Mater.*, 2016, **28**, 4766–4802.

2 (*a*) A. Rogalski, *Infrared Phys. Technol.*, 2002, **43**, 187–210; (*b*) L. Dou, Y. Liu, Z. Hong, G. Li and Y. Yang, *Chem. Rev.*, 2015, **115**, 12633–12665; (*c*) J. Qi, W. Qiao and Z. Y. Wang, *Chem. Rec.*, 2016, **16**, 1531–1548; (*d*) S. P. Singh and G. D. Sharma, *Chem. Rec.*, 2014, **14**, 419–481; (*e*) S. R. Forrest, *Nature*, 2004, **428**, 911–918; (*f*) T. Rauch, M. Boberl, S. F. Tedde, J. Furst, M. V. Kovalenko, G. Hesser, U. Lemmer, W. Heiss and O. Hayden, *Nat. Photonics*, 2009, **3**, 332–336.

3 (*a*) T. M. Clarke and J. R. Durrant, *Chem. Rev.*, 2010, **110**, 6736–6767; (*b*) D. M. Stoltzfus, J. E. Donaghey, A. Armin, P. E. Shaw, P. L. Burn and P. Meredith, *Chem. Rev.*, 2016, **116**, 12920–12955; (*c*) O. Ostroverkhova, *Chem. Rev.*, 2016, **116**, 13279–13415.

4 (*a*) S. H. Park, A. Roy, S. Beaupré, S. Cho, N. Coates, J. S. Moon, D. Moses, M. Leclerc, K. Lee and A. J. Heeger, *Nat. Photonics*, 2009, **3**, 297–302; (*b*) J. J. M. Halls, C. A. Walsh, N. C. Greenham, E. A. Marseglia, R. H. Friend, S. C. Moratti and A. B. Holmes, *Nature*, 1995, **376**, 498–500; (*c*) G. Yu, J. Gao, J. C. Hummelen, F. Wudl and A. J. Heeger, *Science*, 1995, **270**, 1789–1791.

5 T. Wang, M. K. Ravva and J.-L. Brédas, *Adv. Funct. Mater.*, 2016, **26**, 5913–5921.

6 (*a*) R. Noriega, J. Rivnay, K. Vandewal, F. P. Koch, N. Stingelin, P. Smith, M. F. Toney and A. Salleo, *Nat. Mater.*, 2013, **12**, 1038–1044; (*b*) Z. B. Henson, K. Mullen and G. C. Bazan, *Nat. Chem.*, 2012, **4**, 699–704.

7 (*a*) R. C. Coffin, J. Peet, J. Rogers and G. C. Bazan, *Nat. Chem.*, 2009, **1**, 657–661; (*b*) Z. Zhu, D. Waller, R. Gaudiana, M. Morana, D. Mühlbacher, M. Scharber and C. Brabec, *Macromolecules*, 2007, **40**, 1981–1986.

8 (*a*) J. D. Azoulay, Z. A. Koretz, B. M. Wong and G. C. Bazan, *Macromolecules*, 2013, **46**, 1337–1342; (*b*) D. B. Rodovsky, J. Peet, N. Shao, J. D. Azoulay, G. C. Bazan, N. Drolet, Q. Wu and M. Y. Sfeir, *J. Phys. Chem. C*, 2013, **117**, 25955–25960; (*c*) B. F. Wright, K. Sunahara, A. Furube, A. Nattestad, T. M. Clarke, G. C. Bazan, J. D. Azoulay and A. J. Mozer, *J. Phys. Chem. C*, 2015, **119**, 12829–12837.

9 M. E. Foster, B. A. Zhang, D. Murtagh, Y. Liu, M. Y. Sfeir, B. M. Wong and J. D. Azoulay, *Macromol. Rapid Commun.*, 2014, **35**, 1516–1521.

10 (*a*) P. Coppo, H. Adams, D. C. Cupertino, S. G. Yeates and M. L. Turner, *Chem. Commun.*, 2003, 2548–2549; (*b*) P. Coppo and M. L. Turner, *J. Mater. Chem.*, 2005, **15**, 1123–1133; (*c*) N. P. Godman, S. K. Adas, K. M. Hellwig, D. W. Ball, G. J. Balaich and S. T. Iacono, *J. Org. Chem.*, 2016, **81**, 9630–9638; (*d*) B. Pal, W.-C. Yen, J.-S. Yang, C.-Y. Chao, Y.-C. Hung, S.-T. Lin, C.-H. Chuang, C.-W. Chen and W.-F. Su, *Macromolecules*, 2008, **41**, 6664–6671.

11 C. Du, C. Li, W. Li, X. Chen, Z. Bo, C. Veit, Z. Ma, U. Wuerfel, H. Zhu, W. Hu and F. Zhang, *Macromolecules*, 2011, **44**, 7617–7624.

12 (*a*) R. Yang, R. Tian, Q. Hou, W. Yang and Y. Cao, *Macromolecules*, 2003, **36**, 7453–7460; (*b*) G. L. Gibson,

T. M. McCormick and D. S. Seferos, *J. Am. Chem. Soc.*, 2012, **134**, 539–547; (*c*) J. Ohshita, M. Miyazaki, F.-B. Zhang, D. Tanaka and Y. Morihara, *Polym. J.*, 2013, **45**, 979–984; (*d*) J. Song, C. Zhang, C. Li, W. Li, R. Qin, B. Li, Z. Liu and Z. Bo, *J. Polym. Sci., Part A: Polym. Chem.*, 2010, **48**, 2571–2578; (*e*) I. Kmínek, D. Výprachtický, J. Kříž, J. Dybal and V. Cimrová, *J. Polym. Sci., Part A: Polym. Chem.*, 2010, **48**, 2743–2756; (*f*) G. C. Welch, R. C. Bakus, S. J. Teat and G. C. Bazan, *J. Am. Chem. Soc.*, 2013, **135**, 2298–2305.

13 (*a*) L. Pandey, C. Risko, J. E. Norton and J.-L. Brédas, *Macromolecules*, 2012, **45**, 6405–6414; (*b*) C. Risko, M. D. McGehee and J.-L. Brédas, *Chem. Sci.*, 2011, **2**, 1200–1218.

14 J.-L. Brédas, *J. Chem. Phys.*, 1985, **82**, 3808–3811.

15 (*a*) D. Venkateshvaran, M. Nikolka, A. Sadhanala, V. Lemaur, M. Zelazny, M. Kepa, M. Hurhangee, A. J. Kronemeijer, V. Pecunia, I. Nasrallah, I. Romanov, K. Broch, I. McCulloch, D. Emin, Y. Olivier, J. Cornil, D. Beljonne and H. Sirringhaus, *Nature*, 2014, **515**, 384–388; (*b*) A. Troisi and A. Shaw, *J. Phys. Chem. Lett.*, 2016, **7**, 4689–4694.

16 J. Gierschner, J. Cornil and H. J. Egelhaaf, *Adv. Mater.*, 2007, **19**, 173–191.

17 (*a*) J. Mei and Z. Bao, *Chem. Mater.*, 2014, **26**, 604–615; (*b*) H. Chen, J. Peet, S. Hu, J. Azoulay, G. Bazan and M. Dadmun, *Adv. Funct. Mater.*, 2014, **24**, 140–150; (*c*) K. R. Graham, C. Cabanetos, J. P. Jahnke, M. N. Idso, A. El Labban, G. O. Ngongang Ndjawa, T. Heumueller, K. Vandewal, A. Salleo, B. F. Chmelka, A. Amassian, P. M. Beaujuge and M. D. McGehee, *J. Am. Chem. Soc.*, 2014, **136**, 9608–9618; (*d*) A. C. Jakowetz, M. L. Böhm, J. Zhang, A. Sadhanala, S. Huettner, A. A. Bakulin, A. Rao and R. H. Friend, *J. Am. Chem. Soc.*, 2016, **138**, 11672–11679.

18 G. Zotti, G. Schiavon, S. Zecchin, A. Berlin and G. Pagani, *Synth. Met.*, 1994, **66**, 149–155.

19 C. M. Cardona, W. Li, A. E. Kaifer, D. Stockdale and G. C. Bazan, *Adv. Mater.*, 2011, **23**, 2367–2371.

20 T. C. Parker, D. G. Patel, K. Moudgil, S. Barlow, C. Risko, J.-L. Brédas, J. R. Reynolds and S. R. Marder, *Mater. Horiz.*, 2015, **2**, 22–36.

21 Z. Wu, W. Yao, A. E. London, J. D. Azoulay and T. N. Ng, *ACS Appl. Mater. Interfaces*, 2017, **9**, 1654–1660.

22 Y. Zhou, C. Fuentes-Hernandez, J. Shim, J. Meyer, A. J. Giordano, H. Li, P. Winget, T. Papadopoulos, H. Cheun, J. Kim, M. Fenoll, A. Dindar, W. Haske, E. Najafabadi, T. M. Khan, H. Sojoudi, S. Barlow, S. Graham, J.-L. Brédas, S. R. Marder, A. Kahn and B. Kippelen, *Science*, 2012, **336**, 327–332.

23 J. Ajuria, I. Etxebarria, W. Cambarau, U. Munecas, R. Tena-Zaera, J. C. Jimeno and R. Pacios, *Energy Environ. Sci.*, 2011, **4**, 453–458.

24 (*a*) J. D. Zimmerman, V. V. Diev, K. Hanson, R. R. Lunt, E. K. Yu, M. Thompson and S. R. Forrest, *Adv. Mater.*, 2010, **22**, 2780–2783; (*b*) J. D. Zimmerman, E. K. Yu, V. V. Diev, K. Hanson, M. E. Thompson and S. R. Forrest, *Org. Electron.*, 2011, **12**, 869873.

